DIAGNOSIS ON PITTING FAILURE IN GEAR EQUIPMENT USING TIME - FREQUENCY DOMAIN ANALYSIS

YUJI OHUE, Faculty of Engineering, Kagawa University
2217-20, Hayashi-Cho, Takamatsu, 761-0396, Japan
Tel/Fax +81-87-864-2344, E-mail ohue@eng.kagawa-u.ac.jp
TOSHIYA KOUNOU, NOK Co.
KATSUHIKO YAZAMA, Honda Motor Co., Ltd

Abstract: In order to discuss the health monitoring method using time-frequency analysis on the vibration of gear sets, the fatigue test employed for a steel gear pair was carried out using a power circulating gear testing machine. Furthermore, the dynamic characteristics of both steel and sintered gears were measured using a power circulating gear testing machine and were analyzed in a time-frequency domain by the continuous and discrete wavelet transforms. In the case of the failure at the dedendum surface of driven gear, not only the vibration of the gear sets but also the condition of tooth meshing would have to be taken into consideration to diagnose the failed teeth.

Key words: Gear, Diagnosis, Wavelet Transform, Surface Failure, Pitting, Vibration.

INTRODUCTION

In order to make more progress in the gear performance, it is important to evaluate the gear dynamics more precisely, since gear is a main machine element in motion and power transmissions. For preventing the unexpected failure in mechanical systems, a large amount of work has been carried out based on a statistical model developed by Lundberg and Palmgren [1] with reliability models using the classical fatigue theory. However, most of these works did not consider the operating conditions of machine during the fatigue process.

Generally, the gear dynamic performance has been analyzed using Fast Fourier Transform (FFT) as a function of frequency. However, it is difficult to identify an instantaneous change of signals. In many health monitoring applications, it is more useful to analyze how measurement characteristics change as a function of both time and frequency. The Wavelet Transform (WT) is a method for the time-frequency analysis of signals [2, 3]. The WT involves decomposing a signal into a representation comprised of local basis functions called wavelets. Each wavelet is located at a different position on the time axis and is local in the sense that it decays to zero when sufficiently far away form its center. The structure of a non-stationary signal can be analyzed in this way with local features represented by closely-packed wavelets of short length. Therefore, the WT can provide more beneficial information about the frequency compared with the FFT. By reason of the advantage on the WT, the applications of the WT to the diagnostics of the gear sets have been studied [4-7]. Their studies have focused mainly on whether some kinds of the WTs can provide the information to detect the fault of the gear system. However, it is also important to diagnose the failure of the gear sets using not only the WT but also the tooth meshing of the gear pair. Considering the tooth meshing of the gear pair would enable to

construct the new diagnosis for the gear sets, which is different from the conventional diagnosis.

In order to evaluate the dynamic characteristics of gear pair, the dynamic performance of sintered and steel gears were measured using a power circulating gear testing machine. The dynamic characteristics were analyzed in a time-frequency domain by the continuous WT, and also those signals were decomposed and reconstructed by the discrete WT. The validity of the new evaluation method by the WT was discussed. Furthermore, in order to perform the health monitoring of the gear sets, a gear fatigue test was carried out and the dynamic characteristics during the fatigue test were measured and discussed by using the WT.

WAVELET TRANSFORM

The Wavelet Transform (WT) has been extensively developed. Applications of the WT are actively studied in a variety of fields in engineering [4-9]. The Continuous Wavelet Transform (CWT) of a function $f(t)$ is defined as follows.

$$\left(W_\psi f\right)(b,a) = |a|^{-1/2} \int_{-\infty}^{\infty} f(t)\overline{\psi\left(\frac{t-b}{a}\right)}dt \qquad (1)$$

Where, the bar over $\psi(t)$ indicates the conjugate of a mother wavelet function $\psi(t)$, a and b indicate the parameters on frequency and time. The Gabor function defined by Eq. (2) is adopted as the wavelet function $\psi(t)$.

$$\psi(t) = \pi^{-1/4}\left(\frac{\omega_p}{\gamma}\right)^{1/2} exp\left\{-\frac{1}{2}\left(\frac{\omega_p}{\gamma}t\right)^2 + i\omega_p t\right\} \qquad (2)$$

Where, ω_p is a center of angular frequency, γ is a constant and was set at $\pi\,(2/\,ln2)^{0.5} = 5.336$. Figure 1 shows Gabor function based on sinusoidal waves $e^{i\omega t}$ and its Fourier spectrum.

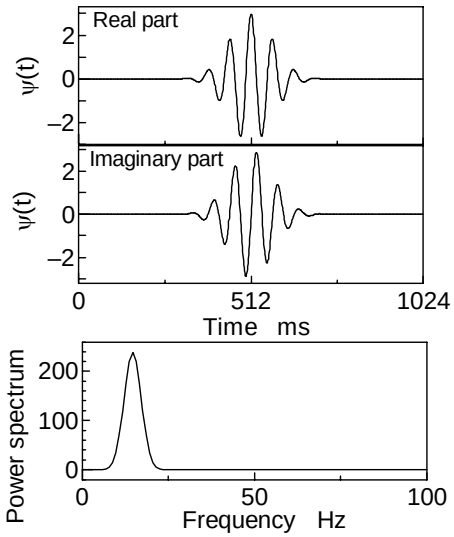

Figure 1. Gabor function.

When the coordinates (b, a) of the CWT shown in Eq.(1) are discretized to the coordinates ($2^{-j}\,k$, 2^{-j}) using two integers j and k, the Discrete Wavelet Transform (DWT) is defined as follows.

$$d_k^{(j)} = 2^{j/2}\int_{-\infty}^{\infty} f(t)\overline{\psi\left(2^j t - k\right)}dt \qquad (3)$$

Where, $d_k^{(j)}$ is equal to $(W_\psi f)(2^{-j}\,k,\ 2^{-j})$. j is called *level*. The Inverse Discrete Wavelet Transform (IDWT) is defined as

$$f(t) \approx \sum_{j=-1} g_j(t) = g_{-1}(t) + g_{-2}(t) + g_{-3}(t) + \cdots \qquad (4)$$

The function $g_j\,(t)$ on the wavelet component is given by

$$g_j(t) = \sum_k d_k^{(j)}\psi\left(2^j t - k\right) \qquad (5)$$

Suppose that $f_j\,(t)$ is the function at a level j, $f_j\,(t)$ is satisfied with the following relation.

$$f_j(t) = \sum_k c_k^{(j)}\phi\left(2^j t - k\right) \qquad (6)$$

Where, $\{c_k^{(j)}\}$ is a sequence at a level j, and $\phi(t)$ is a scaling function. The scaling function $\phi(t)$ and the mother wavelet function $\psi(t)$ are satisfied with the two-scale relations as follows.

$$\phi(t) = \sum_k p_k \phi(2t-k) \tag{7}$$

$$\psi(t) = \sum_k q_k \phi(2t-k) \tag{8}$$

Where, $\{p_k\}$ and $\{q_k\}$ are two-scale sequences. The functions $g_j(t)$ and $f_j(t)$ at a level j are able to be found by using Eqs. (5) and (6). The function $f_j(t)$ decomposed into the function $g_j(t)$ on the wavelet component is satisfied with the following relation.

$$f_j(t) = f_{j-1}(t) + g_{j-1}(t) \tag{9}$$

In this study, the scaling and the mother wavelet functions based on the cardinal B-spline function in order of $m = 4$ was adopted. The cardinal B-spline function $N_m(t)$ in order of m is defined as follows.

$$\phi(t) = N_m(t) = \frac{1}{(m-1)!}\sum_{k=0}^{m}(-1)^k \binom{m}{k}(t-k)^{m-1} \tag{10}$$

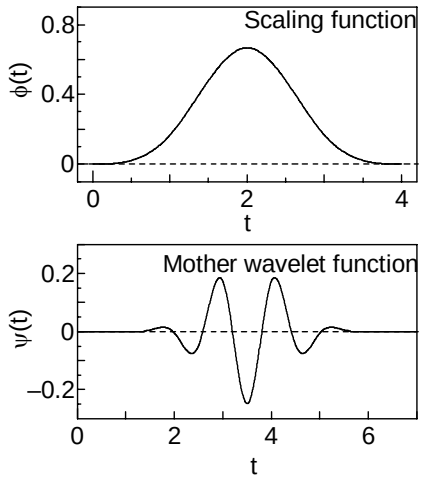

Figure 2. Scaling and wavelet functions ased on Cardinal B-spline in order of 4.

Figure 2 shows the scaling function $\phi(t)$ and the mother wavelet function $\psi(t)$ based on the function $N_4(t)$. The sequences $\{a_k\}$, $\{b_k\}$, $\{p_k\}$ and $\{q_k\}$ are given in Reference [2].

DYNAMIC CHARACTERISTICS

Test Gear and Testing Machine

Table 1 shows the specifications of gear pair employed in this dynamic performance test. The module is 5mm and the pressure angle is 20 deg. The test gears are induction-hardened sintered and chromium molybdenum steel (JIS: SCM440) ones. The mating pinion is case-hardened steel (JIS: SCM415) one. Generally, the sintered materials have higher damping ratio due to the pores, comparing with the steel ones. The density of the sintered gear is 6.9 g/cm^3 [10]. The Young's modulus and Poison's ratio of the sintered gear were 152 GPa and 0.25, and those of the steel gear were 206 GPa and 0.3, respectively.

Table 1. Specifications of gear pair with a center distance of 82.55mm.

		Pinion	Gear
Module	mm	5	
Pressure angle	deg.	20	
Number of teeth		15	16
Addendum modification coefficient		0.571	0.560
Tip circle diameter	mm	90.71	94.6
Center distance	mm	82.55	
Face width	mm	18	6
Contact ratio		1.246	
Accuracy*		Class 1	Class 1
Tooth surface finishing		Grinding	

*JIS B 1702

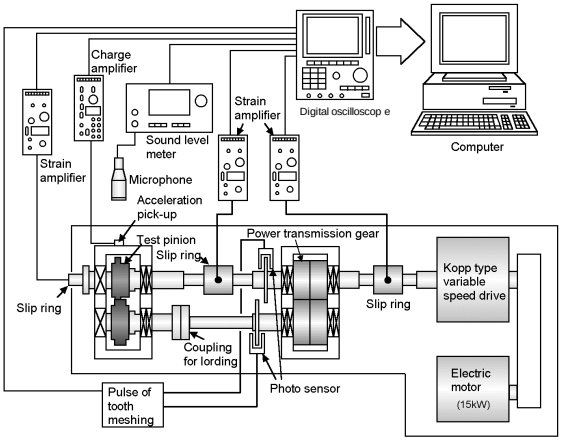

Figure 3. Power circulating gear testing machine.

The test apparatus shown in Fig.3 is a power circulating type gear testing machine with a center distance of 82.55 mm. The test gear was driven within a range of rotational speed n_2 of 1600 rpm to 10000 rpm. The load to the gear pair was statically applied by twisting the gear shaft using a loading lever with dead weights and by fixing using a torsion coupling. The value of the torque was 30 Nm. The lubricating oil was a gear oil with EP additives and was pressure-fed at an oil temperature of 313 K. The vibration acceleration of the gear box was detected by a piezo-electric pickup through an amplifier. The pickup has a maximum response frequency of 20 kHz. These signals were analyzed using a computer and a digital oscilloscope.

Analysis of Gear Dynamics Using WT

Using the DWT and the IDWT, the vibration acceleration of the gear box was decomposed, and was reconstructed in two regions above and below f_z . Figure 4 shows the results of the decomposed vibration acceleration of the gear box at n_2 = 1800 rpm. The level j corresponds to the lower frequency, as the absolute value of j becomes larger. Each function $g_j(t)$ is the wave at each level j including the original wave $f_0(t)$. As the absolute value of level j became larger, the wave shape of $f_j(t)$ became smooth. In this case, level j < -5 corresponds to the frequency band below tooth mesh frequency f_z.

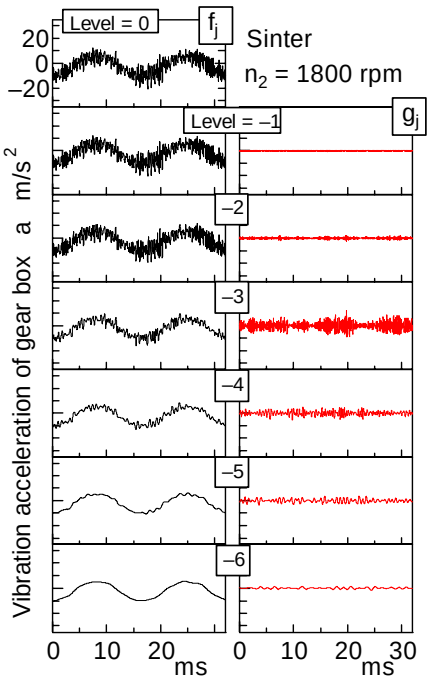

Figure 4. Example of decomposed vibration acceleration of gear box at n_2= 1800rpm.

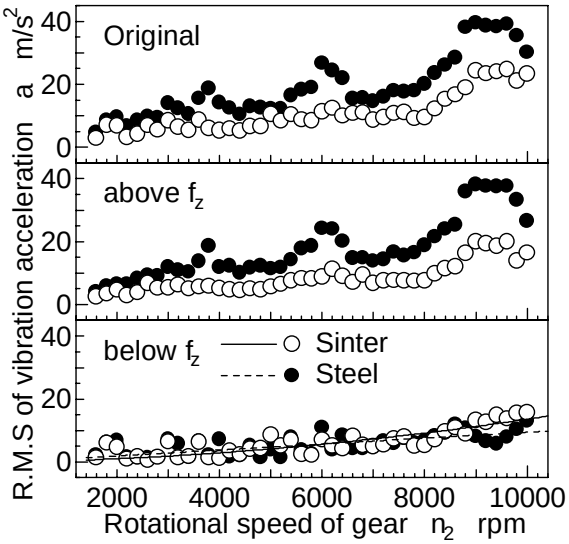

Figure 5. Root mean square of vibration acceleration above and below f_z

Figure 5 shows the root-mean-squares of the vibration acceleration plotted against n_2. The increase in the value of the vibration acceleration reconstructed in the region below f_z is proportional to n_2 to the power two, and is independent of the material of the gear. On the other hand, the values of the vibration acceleration reconstructed in the region above f_z for the sintered gear is smaller than those for

the steel one. This tendency is the same as the behavior of the original vibration acceleration. The vibration due to the tooth mesh propagates to the gear box through shafts and bearings supporting the gear pair. The vibration of the gear box is caused by the torsional vibration of the gear pair due to the tooth mesh. The torsional vibration depends on the frequency components above f_z, since the fluctuations of the vibration are caused by the frequency components above f_z.

HEALTH MONITORING

Fatigue Test

In order to carry out the health monitoring of the tooth surface failure in gear sets, a fatigue test was performed using the gear testing machine shown in Fig. 3. Table 2 shows the specifications of the gear pair. The module is 5 mm and the pressure angle is 20 deg. The test gear pair is case-hardened chromium molybdenum steel one. The center distance of the test gear pair is 102mm. The fatigue test was carried out at a rotational speed of 1800 rpm for the pinion.

Table 2. Specifications of gear pair with a center distance of 102mm.

		Pinion	Gear
Module	mm	5	
Standard pressure angle	deg.	20	
Number of teeth		20	21
Addendum modification coefficient		0	-0.19
Tip circle diameter	mm	110	113.1
Center distance	mm	102	
Face width	mm	5	22
Contact ratio		1.54	
Accuracy*		Class 2	Class 2
Heat treatment		Case-hardening	
Tooth surface finishing		Grinding	Shot-peening

*JIS B 1702

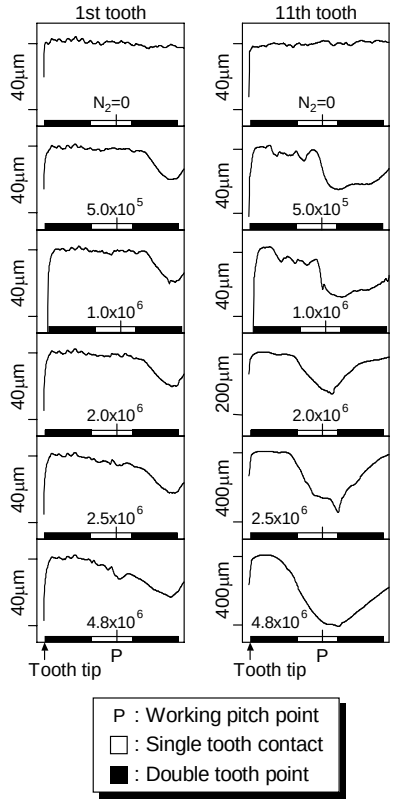

(a) Pinion tooth No. 1 (b) Pinion tooth No. 11

Figure 6. Tooth profile error of pinion during fatigue test.

Figures 6 and 7 show the tooth profile errors of the test gear pair and the observations of the tooth surfaces of the pinion tooth No.1 and No.11 during the fatigue process under a maximum Hertzian stress of p_{max} = 1850 MPa at the pitch point of the gear pair. The test pinion was failed by pitting at a number of fatigue cycles of $N_2 = 4.8\text{x}10^6$. At $N_2 = 0$, before the fatigue test, the tooth profiles of both the gear and the pinion are considerably smooth. As the number of stress cycles increases up to $N_2 = 1.0\text{x}10^6$, the dedendum tooth of the pinion wears due to the interference between the dedendum tooth of the pinion and the mating gear. While, at $N_2 = 2.0\text{x}10^6$, the tooth profile of the pinion tooth No.11 changes at the dedendum tooth. This change of the tooth profile depends on the pitting shown in Fig. 7. Finally, the maximum tooth profile error of the pinion tooth No.11

reaches about 400 μm. However, the tooth profile error of the pinion tooth No.1 is only about 20 μm. The maximum tooth profile errors of pinion having 20 teeth, at each fatigue stage. Each tooth profile error is less than 40 μm up to N_2 = 1.0x10^6. At N_2 = 2.0x10^6, the tooth profile error of tooth No.11 becomes larger than those of the other ones, and the values are about 150 μm. At N_2 = 4.8x10^6, the tooth profile errors of the tooth No.11, No.12 and No.15 become larger. The toot profile of the mating gear during the fatigue test does not change remarkably.

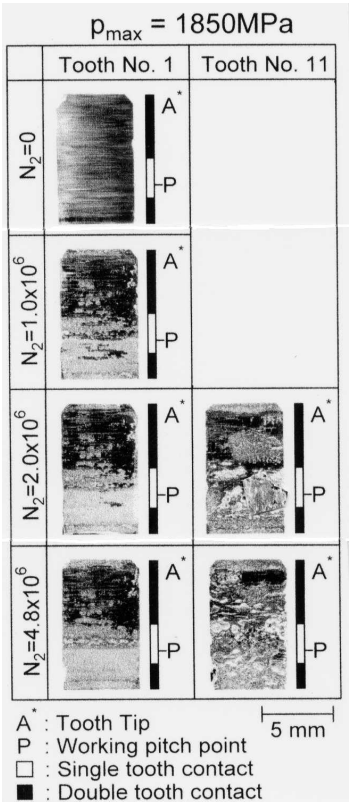

Figure 7. Observation of pinion teeth

Health Monitoring

Figure 8 shows the vibration acceleration of the gear box, its WT map and FFT spectrum at (a) N_2 = 0 and (b) N_2 = 2.0x10^6. In this fatigue test, the tooth mesh frequency f_z is 600 Hz. At both the fatigue stages, it is difficult to diagnose the tooth surface failure only by the vibration acceleration waves. Comparing the FFT spectrum at N_2 = 2.0x10^6 with that at N_2 = 0, it is understood that the tooth surface failure occurred at N_2 = 2.0x10^6, since the intensity of the frequencies except for tooth mesh frequency f_z and its harmonic frequencies became larger at N_2 = 2.0x10^6. From the result of WT map at N_2 =0, it is understood that the intensities at tooth mesh frequency f_z and its harmonic frequencies during the one rotation of the pinion are not constant but fluctuate against the time. At the moment when each tooth pair meshes, the intensities at the tooth mesh frequency f_z and its harmonic frequencies increase. The WT map at N_2 = 2.0x10^6 shows that the intensities at tooth mesh frequency f_z and its harmonic frequencies near the meshing of tooth No.11 increase. It is considered that the changes in those intensities are caused by the deterioration of tooth No.11 due to pitting.

The tooth profile deterioration caused the change of the intensities at tooth mesh frequency and its harmonic frequencies. Therefore, the health monitoring was carried out by the vibration acceleration having the component of tooth mesh frequency f_z. The vibration acceleration having the component of f_z can be calculated using DWT. Figure 9 shows the decomposed vibration acceleration of the gear box at (a) N_2 = 0 and (b) N_2 = 2.0x10^6. The level j corresponds to the lower frequency, as the absolute value of j becomes larger. The vibration due to the tooth mesh propagates to the gear box through shafts and bearings supporting the gear pair. Therefore, comparing the decomposed result at N_2 = 0 with that at N_2 = 2.0x10^6, the amplitude of the decomposed vibration acceleration near meshing of tooth No.11 becomes larger. This result corresponds with the result of the WT map shown in Fig. 8. However, since the discrete WT can provide the signal with the component of tooth mesh frequency, the discrete WT is superior to the continuous WT.

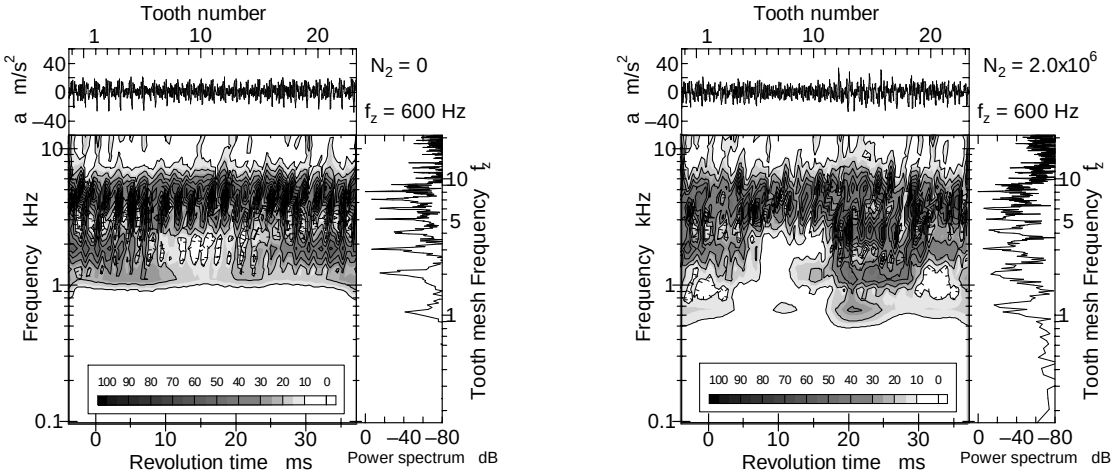

Figure 8. Vibration acceleration of gear box , its WT map and FFT spectrum during fatigue test.

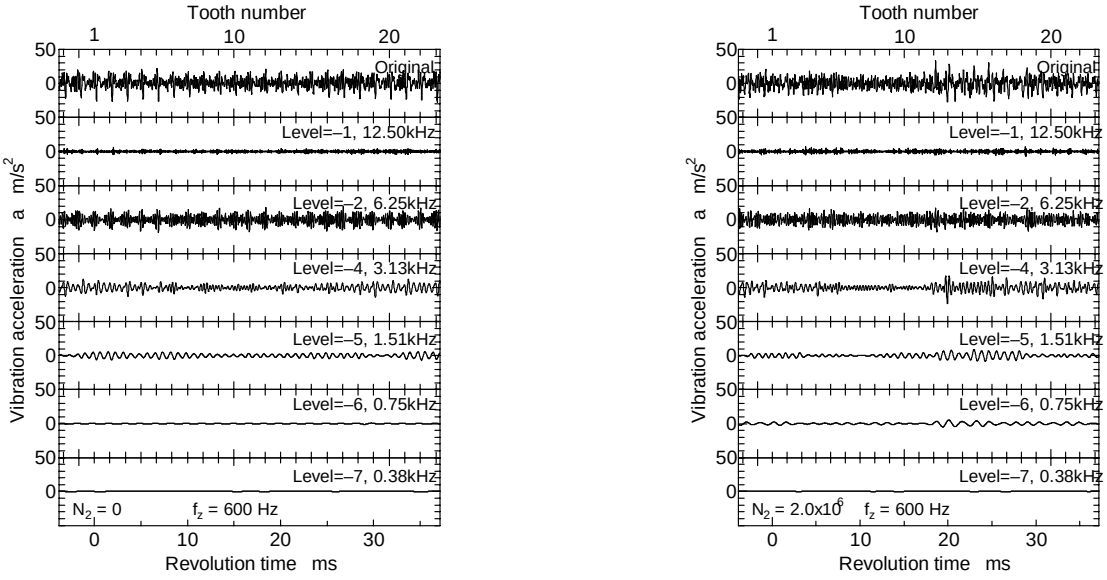

Figure 9. Decomposed vibration acceleration of gear box during fatigue test

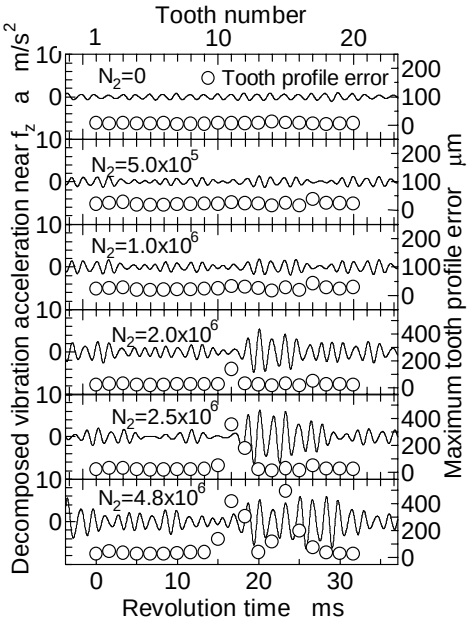

Figure 10. Relation between vibration acceleration and maximum tooth profile during fatigue test.

Since the vibration acceleration of the gear box is caused by tooth meshing, the fundamental frequency of the vibration acceleration of the gear box is tooth mesh frequency f_z. Therefore, the relationship between the vibration acceleration having the component of tooth mesh frequency f_z and the maximum tooth profile error was investigated during the fatigue test. The relationship is shown in Figure 10. In this case, the vibration acceleration having the component of a frequency of 750Hz was adopted since the tooth mesh frequency f_z is 600 Hz. The tooth profile error of each tooth at $N_2 = 0$ is less than those at $N_2 = 5.0 \times 10^5$ and 1.0×10^6. Therefore, the amplitude of the vibration acceleration having tooth mesh frequency becomes slightly larger from $N_2 = 5.0 \times 10^5$ to 1.0×10^6. The dedemdum surface of the tooth No.11 was failed by pitting and the maximum tooth profile error of the tooth No.11 is larger than those of the other teeth at $N_2 = 2.0 \times 10^6$. However, the amplitude of the vibration acceleration becomes maximum, not at the meshing point of tooth No. 11, but after the meshing point of tooth No. 12. The pitting failure in the pinion occurred the tooth surface near the pitch point, but the addendum tooth surface of the pinion did not fail and was smooth as shown in Fig. 6. When the driven pinion meshes with the mating gear, the tooth mesh starts from the addendum surface of the pinion. At the beginning of the meshing of tooth No.11, the smooth dedendum surface of tooth No.10 and the smooth addendum surface of tooth No.11 mesh with each mating gear tooth. While, at the beginning of the meshing of tooth No.12, the failed dedemdum surface of tooth No.11 and the smooth addendum surface of tooth No.12 mesh with each mating gear tooth. It can be considered from the above evidence that the impact force due to the meshing of tooth No.12 is much larger than that due to the meshing of tooth No.11. Therefore, it is understood that the amplitude at the meshing of tooth No.11 is smaller than that at the meshing of tooth No.12. In this case of the failure at the dedendum surface of driven gear, the amplitude of the vibration acceleration with the component of tooth mesh frequency became larger after the failed tooth meshing. Therefore, not only the vibration of the gear sets but also the condition of tooth meshing would have to be taken into consideration to diagnose the failed teeth. At $N_2 = 4.8 \times 10^6$, since the teeth profiles of tooth No.10 to No.16 deteriorate comparing with the others, the amplitude of the vibration acceleration fluctuates widely during the meshing of those teeth. From the above result, the proposed method in this paper, which is to monitor the vibration with the component of tooth mesh frequency f_z, makes it possible to discuss the health monitoring of the gear sets more precisely than the previous papers.

CONCLUSION

In order to evaluate the dynamic characteristics of gear pair, the dynamic performance were analyzed by the WT. The validity of a evaluation method by the WT was discussed. Furthermore, to perform the health monitoring, a gear fatigue test was carried out and the dynamic characteristics during the

fatigue test were analyzed. The main results are summarized as follows.

(1) The behavior of the vibration acceleration of the gear box against the rotational speed of the gear could be divided to two different behaviors above and below f_z. The behavior of the vibration acceleration below f_z was independent of the gear material and was proportional to the rotational speed to the power two. The behavior of the vibration acceleration above f_z was influenced by the difference in the gear material.
(2) A failed tooth by pitting could be found out by the intensity of the vibration acceleration having the tooth mesh frequency f_z on the wavelet map during fatigue process. Furthermore, the wave shape of the vibration acceleration having the tooth mesh frequency f_z could be analyzed using the discrete wavelet transform. The mesh condition of the gear pair with failed tooth could be gained from the amplitude of the vibration acceleration having the tooth mesh frequency f_z.
(3) The proposed method in this paper is to monitor the vibration of gear sets having the component of tooth mesh frequency f_z using the wavelet transform, and evaluate the damage of the gear tooth from the change in the amplitude of the vibration having the frequency f_z. In the case of the dedendum surface failure of driven gear, however, the vibration acceleration with the component of tooth mesh frequency became larger after the failed tooth meshing.

ACKNOWLEDGEMENT

The authors would like to thank Sumitomo Metal Industries, Ltd. and Japan Energy Co. Ltd. for providing materials and lubricating oil. This research was supported by the Grants-in-Aid for Scientific Research of JSPS.

REFERENCES

[1] Lundberg, G. and Paqlmgren, A., Dynamic capacity of Rolling Bearings, *ACTA, Polytechnica, Mechanical Engineering Series*, Vol. 1, No. 3, 1947.
[2] Chui, C. K., Introduction to Wavelet, *Academic Press*, 1992.
[3] Mallat, S., A Wavelet Tour of Signal Processing, *Academic Press*, 1998.
[4] Staszewski, W. J. and Tomlinson, G. R., Application of the Wavelet Transform to Fault Detection in a Spur Gear, *Mechanical Systems and Signal Processing*, 8(3), 1994, pp. 289-307.
[5] Wang, W. J. and McFadden, P. D., Application of Wavelets to Gearbox Vibration Signals for Fault Detection, *Journal of Sound and Vibration*, 192(5), 1996, pp. 927-939.
[6] Paya, B. A., Esat, I. I. and Badi, M. N. M., Artificial Neural Network Based Fault Diagnostics of Rotating Machinery Using Wavelet Transforms as a Preprocessor, *Mechanical Systems and Signal Processing*, 11(5), 1997, pp. 751-765.
[7] Yoshida, A., Ohue, Y., A Study on Diagnosis of Tooth Surface Failure by Wavelet Transform of Dynamic Characteristics, *Proc. 5th International Tribology Conference in Australia*, 1998, pp. 11-16.
[8] Qian, S. and Chen, D., Joint Time-Frequency Analysis, *Prentice Hall PTR*, 1996.
[9] Ding, Y. , Reuben, R. L. , Steel, J. A. , A New Method for Waveform Analysis for Estimating AE Wave Arrival Times Using Wavelet Decomposition, NDT & E International, Vol. 37, No. 4, 2004, pp. 279 - 290
[10] Yosida, A., Ohue, Y. and Karasuno, I., Surface Failure and Durability of Induction-Hardened Sintered Powder Metal Rollers and Gears with Various Hardened Depths, *Transactions of the ASME, Journal of Mechanical Design*, Vol. 116, 1994, pp. 730-737.